Cytotoxic T Cells Use Mechanical Force to Potentiate Target Cell Killing

Roshni Basu, Benjamin m. Whitlock, Julien Husson, Audrey Le floc'h, Weiyang Jin, Alon Oyler-Yaniv, Farokh Dotiwala, Gregory Giannone, Claire Hivroz, Nicolas Biais, et al.

HHS Public Access

Author manuscript

Cell. Author manuscript; available in PMC 2017 March 24.

Published in final edited form as:

Cell. 2016 March 24; 165(1): 100–110. doi:10.1016/j.cell.2016.01.021.

Cytotoxic T cells use mechanical force to potentiate target cell killing

Roshni Basu[1,¶], **Benjamin M. Whitlock**[2,¶], **Julien Husson**[3,¶], **Audrey Le Floc'h**[1], **Weiyang Jin**[4], **Alon Oyler-Yaniv**[5], **Farokh Dotiwala**[6], **Gregory Giannone**[7], **Claire Hivroz**[8], **Nicolas Biais**[9], **Judy Lieberman**[6], **Lance C. Kam**[4], and **Morgan Huse**[1,*]

1

2

3

4

5

6

7

8

9

SUMMARY

The immunological synapse formed between a cytotoxic T lymphocyte (CTL) and an infected or transformed target cell is a physically active structure capable of exerting mechanical force. Here, we investigated whether synaptic forces promote the destruction of target cells. CTLs kill by secreting toxic proteases and the pore forming protein perforin into the synapse. Biophysical experiments revealed a striking correlation between the magnitude of force exertion across the synapse and the speed of perforin pore formation on the target cell, implying that force potentiates cytotoxicity by enhancing perforin activity. Consistent with this interpretation, we found that increasing target cell tension augmented pore formation by perforin and killing by CTLs. Our data also indicate that CTLs coordinate perforin release and force exertion in space and time. These results reveal an unappreciated physical dimension to lymphocyte function and demonstrate that cells use mechanical forces to control the activity of outgoing chemical signals.

*Correspondence: husem@mskcc.org (M.H.).
¶Equal contribution.

Author Contributions

R.B., B.M.W., J.H., A.L.F., W.J., A.O.-Y., N.B., L.C.K., and M.H. designed the experiments. R.B., B.M.W., J.H., A.L.F., W.J., A.O.-Y., and M.H. collected the data. R.B., B.M.W., J.H., A.L.F., A.O.-Y., and M.H. analyzed the data. F.D. and J.L. provided assistance with purified perforin. G.G. and C.H. contributed key insights. M.H., R.B., and L.C.K. wrote the manuscript.

INTRODUCTION

Cells exchange information through adhesive and highly dynamic cell-cell interactions. Within these contacts, communicative chemical processes are exposed to micrometer scale membrane and cytoskeletal movements capable of imparting substantial mechanical force. It is known that cells use applied force to sense the physical properties of their environment and translate this information into afferent chemical signals that flow into the cell. This process, called mechanotransduction, plays critical roles in the activation and differentiation of multiple cell types (Ingber, 2006; Orr et al., 2006). In principle, force could also modulate intercellular communication, particularly in close cell-cell interactions where movement on one side of the interface induces physical changes on the other side. Whether cell-derived forces actually contribute to the transmission of efferent signals in this manner, however, remains unclear.

Cell-cell contacts in the immune system represent an interesting experimental context for exploring this question because they are structurally dynamic and also mediate a substantial amount of information transfer. One of the most important of these interactions is the immunological synapse (IS) used by cytotoxic T lymphocytes (CTL) to instruct infected or transformed target cells to die. Target cell killing is crucial for adaptive immune responses against intracellular pathogens, and it also plays a central role in several cell-based anti-cancer immunotherapies (Grupp and June, 2011). IS assembly is triggered by the recognition of cognate peptide-major histocompatibility complex (pMHC) on a potential target by T cell receptors (TCRs) on the CTL. Once the IS forms, CTLs secrete a toxic mixture of proteins into the synaptic space that includes perforin and several granzyme proteases (Stinchcombe and Griffiths, 2007). Perforin is a hydrophobic molecule that forms calcium (Ca^{2+})-dependent pores in the target cell membrane. This induces a repair response that enables granzymes to access the target cell cytoplasm, where they induce apoptosis (Keefe et al., 2005; Thiery et al., 2011).

Perforin and granzymes are stored in secretory lysosomes called lytic granules, which cluster around the centrosome in activated CTLs. During IS formation, the centrosome reorients to the center of the contact, placing the granules in close apposition to the synaptic membrane (Stinchcombe et al., 2006). This polarization event is thought to enhance the potency and the specificity of killing by promoting directional release of granule contents toward the target. Recent results, however, indicate that CTLs kill quite effectively in the absence of centrosome reorientation (Bertrand et al., 2013), suggesting there are additional mechanisms by which the IS potentiates cytotoxicity.

IS formation also involves intense remodeling of filamentous actin (F-actin), which controls both the growth and the organization of the interface (Le Floc'h and Huse, 2015). Recently, we demonstrated that phosphoinositide 3-kinase (PI3K) activity stimulates actin polymerization within the IS by recruiting Dock2, an exchange factor for the Rho GTPase Rac (Le Floc'h et al., 2013). CTLs lacking Dock2 form miniaturized synapses that are structurally unstable. Conversely, depletion of PTEN, a lipid phosphatase that antagonizes PI3K, markedly enhances IS growth. Interestingly, whereas Dock2 deficient CTLs kill target cells poorly, PTEN deficient CTLs exhibit dramatically enhanced cytotoxicity (Le Floc'h et

al., 2013). These results establish an intriguing link between target cell killing and F-actin remodeling at the IS. The mechanistic basis for this relationship, however, has remained unclear.

Synaptic F-actin is highly dynamic, exhibiting constant retrograde flow toward the center of the IS as well as bursts of anterograde flow in the opposite direction (Bunnell et al., 2001; Grakoui et al., 1999; Ritter et al., 2015). These and other effects enable the T cell to impart nanonewton scale forces against the target cell (Bashour et al., 2014; Husson et al., 2011). In the present study, we combined specific perturbations of PI3K-Dock2 signaling with single cell biophysical approaches to investigate the impact of synaptic forces on CTL function. We found that force exertion at the IS potentiates killing by straining the target cell surface and thereby enhancing the pore forming activity of perforin. These results demonstrate that T cells mix physical and chemical outputs to enhance their effector responses and reveal an unexpected role for cellular mechanics in intercellular communication.

RESULTS

Cytotoxicity correlates with synaptic force exertion

The killing phenotypes observed in PTEN and Dock2 deficient CTLs implied an important role for PI3K dependent F-actin remodeling in cellular cytotoxicity. To investigate this relationship, we first examined the distribution of lytic granules in CTL-target cell conjugates. CTLs expressing the OT1 TCR, which recognizes the ovalbumin$_{257–264}$ peptide (OVA) bound to the class I MHC molecule H2-K^b, were transduced with shRNA against PTEN (shPTEN) or Dock2 (shDock2) or with nontargeting control shRNA (shNT) (Figure S1, available online). They were then mixed with OVA-loaded EL4 target cells and the resulting conjugates fixed and stained to visualize lytic granules (Figure 1A). Suppression of Dock2 or PTEN had no effect on granule polarization to the IS (Figure 1B), indicating that intracellular trafficking of cytotoxic cargo does not involve PI3K-Dock2 signaling. We also quantified granule release (called degranulation) from CTLs by measuring surface exposure of the granule resident protein Lamp1 after stimulation with target cells. This response was unaffected by depletion of PTEN or Dock2 (Figure 1C), consistent with previous results (Le Floc'h et al., 2013). Finally, we examined TCR-induced calcium (Ca^{2+}) flux, a requisite step for granule clustering and exocytosis (Beal et al., 2009; Ostergaard et al., 1987), by imaging CTLs on glass surfaces coated with H2-K^b-OVA and ICAM1 (a ligand for the $\alpha_L\beta_2$ integrin LFA1). Dock2 and PTEN deficient CTLs displayed robust Ca^{2+} responses that were comparable to those of shNT expressing controls (Figure 1D–E). Taken together, these data indicate that suppression of PTEN and Dock2 does not affect granule polarization and fusion at the IS, implying that these perturbations influence cytotoxicity via a different mechanism.

Force exertion across the IS could, in principle, provide a physical avenue for control of target cell killing. To investigate this possibility, we first asked whether PI3K-Dock2 signaling, which controls cytotoxic efficiency, might also regulate IS mechanics. Accordingly, we compared synaptic force exertion in OT1 CTLs transduced with shNT, shPTEN, and shDock2. To measure forces perpendicular to the IS, we used micropipettes to place individual CTLs in contact with polystyrene beads coated with H2-K^b-OVA and ICAM1 (Figure 2A). Subsequent bead displacements toward or away from the CTL were

translated into force measurements using the known stiffness of the micropipette holding the bead (see Experimental Procedures). Contact with stimulatory beads induced a rapid CTL spreading response not unlike IS formation with a target cell. Spreading was frequently accompanied by transient pushing of the bead away from its initial position. This was followed in almost all cases by a pronounced pulling phase in which the bead became engulfed by the CTL (Figure 2B, Movie S1 available online). Analysis of kymographs derived from each experimental trial enabled us to determine the rate of bead movement during the pulling phase of the response (Figure 2C), which is proportional to the pulling force. This parameter, called the loading rate, was significantly enhanced in CTLs lacking PTEN and markedly reduced in CTLs lacking Dock2 (Figure 2D). These results indicate that PI3K-Dock2 signaling drives force exertion perpendicular to the CTL-target cell interface.

To measure forces in the plane of the IS, we imaged OT1 CTLs on arrays of polydimethylsiloxane (PDMS) micropillars bearing immobilized H2-K^b-OVA and ICAM1 (Figure 3A) (Bashour et al., 2014). Because the dimensions (6 μm tall, 0.7 μm diameter) and composition of these pillars were known, observed pillar deflections could be converted into force vectors. OT1 CTLs exhibited cell spreading and OVA-induced Ca^{2+} flux upon contact with the arrays, consistent with canonical TCR activation and signaling (Figure 3B, Figure S2A). In most cells, spreading was associated with centrifugal pillar deflections, indicative of outwardly oriented forces (Figure 3B–C, Movie S2). After the size of the interface stabilized, these deflections tended to reverse polarity and point inward. The progression from centrifugal “spreading” to centripetal “squeezing” was reminiscent of the responses displayed by naive $CD4^+$ T cells on pillar arrays (Bashour et al., 2014). However, OT1 CTLs exerted substantially more force per pillar than naïve cells (Figure 3D) (Bashour et al., 2014), and their force profiles were less symmetric. Indeed, instantaneous force exertion tended to be concentrated in “hotspots” characterized by the strong deflection of 1–3 pillars (Figure 3B, green asterisks). Importantly, suppression of PTEN markedly enhanced force exertion on both individual pillars and also the entire array (Figure 3E, Figure S2B). Dock2 suppression gave less conclusive results, with some experiments revealing a slight inhibitory effect and others indicating no significant difference (Figure 3F, Figure S2B). It is possible that forces in the plane of the IS are less sensitive to reduced PI3K signaling than those in the orthogonal dimension. Nevertheless, when taken together with our micropipette data, these studies indicate that CTLs exert multidimensional PI3K dependent forces against the target cell.

Myosin-based contractility is crucial for the generation of actin dependent forces in multiple cell types, and clusters of the nonmuscle myosin II (NMII) isoform have been observed within the T cell IS (Babich et al., 2012; Jacobelli et al., 2004; Yi et al., 2012). Although the precise function of synaptic NMII remains controversial (Hammer and Burkhardt, 2013), it is appropriately positioned to contribute to force exertion. To investigate this possibility, we examined micropillar deflection in the presence of blebbistatin, a small molecule myosin II inhibitor. Blebbistatin treatment dramatically reduced force exertion during both the “spreading” and “squeezing” phases of the response (Figure 3G, S2C), indicative of an important role for NMII in IS mechanics. Next, we asked whether synaptic force exertion by NMII modulates cytotoxicity. For these experiments, we utilized shRNA knockdown of the

myosin heavy chain MyH9 (shMyH9) to target the NMII complex selectively in CTLs. This strategy yielded only partial suppression of MyH9 (Figure S2D), as previously reported (Liu et al., 2013). CTLs expressing shMyH9 exhibited a subtle, but consistent killing defect that paralleled the partial knockdown of the protein (Figure 3H). Importantly, TCR-induced degranulation was not inhibited in these cells (Figure S2E), indicating that TCR activation and signaling remained intact. We conclude that myosin activity, like PI3K signaling, controls both cytotoxicity and synaptic force exertion.

PI3K signaling accelerates perforin pore formation

Next, we re-examined how PI3K signaling affects cytotoxicity, focusing on events that occur downstream of perforin and granzyme secretion. Perforin initiates killing by forming plasma membrane pores on the target cell (Pipkin and Lieberman, 2007). This event can be visualized by imaging CTLs and target cells in the presence of high concentration (100 μM) propidium iodide (PI) (Keefe et al., 2005; Lopez et al., 2013). Plasma membrane perforation allows PI to access the cytoplasm, rendering the target cell fluorescent (Figure 4A). To quantify the rate of perforin pore formation using this approach, we imaged OVA-loaded RMA-s target cells together with OT1 CTLs in 50×50 μm PDMS microwells, which facilitate extended observation of individual CTL-target cell interactions (Figure 4B, Movie S3). These experiments revealed that CTLs expressing shPTEN were significantly more effective at inducing perforin pore formation than shNT expressing controls. The fraction of interactions associated with target cell PI incorporation was higher (93% for shPTEN CTLs vs. 71% for shNT CTLs), and among these the time delay between IS formation and PI fluorescence (influx time) was significantly reduced (Figure 4C).

CTLs lacking PTEN exhibited higher total levels of perforin protein (Figure 4D), which could, in principle, explain the enhanced pore formation we observed. This increase in perforin expression could be reversed, however, by removing one copy of the *prf1* gene in the context of PTEN deficiency. Importantly, killing by PTEN deficient $prf1^{+/-}$ CTLs was essentially equivalent to that of PTEN deficient $prf1^{+/+}$ CTLs and substantially greater than that of $prf1^{+/+}$ shNT controls (Figure 4E). Hence, it is unlikely that the accelerated pore formation seen in the absence of PTEN resulted from changes in perforin expression. Rather, PTEN suppression appeared to boost cytotoxicity by increasing perforin activity on a per molecule basis.

Cell tension potentiates target cell lysis

Biophysical studies have shown that increasing the tension of target membranes boosts the activity of pore forming peptides, implying that tangential force can reduce the energetic cost of inserting a hydrophobic molecule into the bilayer (Huang et al., 2004; Lee et al., 2008; Polozov et al., 2001). Accordingly, we reasoned that synaptic forces might potentiate perforin pore formation by applying tension to the target cell. To explore the relationship between cell tension and perforin function, we grew adherent cells on polyacrylamide hydrogels of varying elasticity (Engler et al., 2006). Cell tension in this culture system mirrors the underlying hydrogel; stiff hydrogels enforce high tension, while soft hydrogels induce the opposite effect (Chan and Odde, 2008; Hui et al., 2015; Lo et al., 2000; Oakes et al., 2009). Consistent with this principle, we found that B16 melanoma cells adopted a

stellate architecture on stiff (E = 50 kPa) hydrogels characteristic of high tension, while on soft (E = 12 kPa) hydrogels they displayed a more collapsed morphology (Figure S3). To assess perforin pore formation under each condition, we treated the cells with purified perforin protein (~ 1 μg/ml) in the presence of 100 μM PI (Figure 5A). Although the capacity of perforin to induce PI influx varied from day to day (see Supplemental Experimental Procedures), we consistently observed that cells on 50 kPa substrates were more sensitive to pore formation than those on 12 kPa substrates, implying that increased cell tension potentiates perforin activity (Figure 5B–C, Figure S4A, Movies S4 and S5).

Next, we investigated whether target cell tension similarly modulates CTL-mediated killing. OT1 CTLs were added to OVA-loaded B16 cells grown on stiff or soft substrates, and target cell lysis measured by the release of lactate dehydrogenase (LDH), a cytoplasmic enzyme (Figure 5D). Killing was significantly enhanced on 50 kPa hydrogels relative to 12 kPa hydrogels, despite equivalent levels of TCR-induced degranulation (Figure 5E, S5). Importantly, target cell killing by the small molecule staurosporine, which induces apoptosis in multiple cell types, was unaffected by substrate elasticity (Figure 5F–G). B16 cells grown on stiff matrices are therefore not intrinsically less viable. Rather, they are selectively sensitized to perforin dependent killing.

Cell tension is imposed both by the cytoskeletal cortex and by the plasma membrane. To determine the relative contributions of membrane and cortical tension to perforin function, we assessed pore formation in the presence of reagents that alter the two parameters differentially (Figure 6A). Blebbistatin, by inhibiting myosin II, reduces cortical tension while increasing membrane tension (Houk et al., 2012; Lee et al., 2011). By contrast, the actin depolymerization agent latrunculin A reduces both parameters (Masters et al., 2013; Wakatsuki et al., 2001). Treatment of adherent B16 cells with latrunculin A substantially decreased pore formation by purified perforin, while blebbistatin reproducibly enhanced it (Figure 6B, Figure S4B–C). These results suggested that membrane tension, rather than cortical tension, controls perforin activity. To further test this idea, we treated cells with hypotonic and hypertonic buffers, which increase and decrease, respectively, membrane tension (Houk et al., 2012) (Figure 6C). Pore formation was enhanced by hypotonic buffer and suppressed by hypertonicity (Figure 6D, Figure S4D), further supporting the idea that perforin and membrane tension function synergistically.

Synaptic force exertion is coordinated with degranulation

Finally, we examined whether perforin release is spatiotemporally correlated with the application of force at the IS, using a degranulation probe containing a pH sensitive GFP (pHluorin) attached to the C-terminal domain of Lamp1 (Rak et al., 2011). pHluorin-Lamp1 is sorted into lytic granules, where its fluorescence is quenched by the acidic environment. Granule fusion with the plasma membrane, however, neutralizes the pH around the pHluorin, allowing it to fluoresce. When CTLs expressing pHluorin-Lamp1 were imaged on PDMS micropillars coated with H2-K^b-OVA and ICAM1, degranulation events appeared as abrupt increases in green fluorescence within the interface between the CTL and the array (Figure 7A–B). Most events occurred within 5 min of initial contact (Figure 7C), and many seemed to be closely associated with hotspots of strong force exertion (Figure 7D).

To quantify the relationship between degranulation and force, we computed the distance between each granule fusion event and the closest pillar experiencing strong deflections during that time (called the Distance to Displaced Pillar (DDP), see Experimental Procedures). We then compared each value to a null distribution generated by performing the DDP calculation for every xy position within the interface between the CTL and the array (Figure 7E). DDP values associated with degranulation events were significantly lower than the mean values of their paired null distributions, indicating that the observed coupling between granule release and pillar deflection did not occur by chance (Figure 7F). We also quantified the radial distribution of degranulation and force exertion within the IS (Figure 7G), and found that both parameters were enriched within an annular region slightly more than halfway between the center of the IS and its outer edge (Figure 7H–I). Taken together, these results suggest that CTLs spatiotemporally coordinate cytolytic secretion with the local application of force, and they also identify a domain within the IS in which these interactions occur.

Could forces within this degranulation zone apply enough membrane tension to potentiate perforin pore formation? To address this question, we first determined the membrane tension change necessary to sensitize a cell to perforin. Using an established approach in which an optical trap is used to pull a thin tether of membrane from the cell surface (Dai and Sheetz, 1995) (Figure S6A–B), we calculated the membrane tension of adherent B16 cells to be 100 μN/m. In the presence of latrunculin A, which protects cells from perforin pore formation (Figure 6B and Figure S4B), membrane tension decreased to 15 μN/m. These data suggest that a ~85 μN/m difference in membrane tension (equivalent to 85×10^{-18} J/μm^2) is sufficient to make perforin pore formation more energetically favorable (Figure S6C). Assuming a pore size of 15 nm, this tensional difference implies a free energy change of 1.5×10^{-20} J per pore (see Experimental Procedures). In micropillar experiments, we routinely observed pillar deflections of > 1 μm within force exertion hotspots. Each of these strong deflections required > 340 pN of force (Figure 3D), implying the transfer of > 170×10^{-18} J of mechanical energy (see Experimental Procedures) within a ~1 μm^2 region of the array. This degree of energy transmission (170×10^{-18} J/μm^2) compares favorably with the tensional change (85×10^{-18} J/μm^2) demonstrated by the tether experiments to modulate perforin activity, and it would be sufficient, in principle, to mechanically potentiate a large number of pores. Hence, under conditions of close synaptic contact, CTLs should be capable of locally sensitizing the target cell membrane to perforin.

DISCUSSION

Communication between immune cells is generally presented as a chemical process based on ligand recognition by receptors. It is becoming increasingly clear, however, that mechanical forces at cell-cell interfaces are necessary both to enable and to regulate communicative chemical interactions. Recent studies have documented the importance of cytoskeletally driven pulling for receptor activation and antigen uptake (Comrie et al., 2015; Liu et al., 2014; Natkanski et al., 2013), which are both processes that mediate information flow into the lymphocyte. Our results demonstrate that physical forces can also modulate information flow out of the cell, in this case by potentiating the activity of a secreted protein, perforin. This synergy between applied force and outgoing chemical signals, which we term

mechanopotentiation, conceptually expands the purview of cellular mechanics as an active mediator of not only afferent but also efferent intercellular communication.

It has been proposed that the IS enhances the intensity and specificity of intercellular communication by restricting the diffusion of secreted factors (Huse et al., 2006; Stinchcombe and Griffiths, 2007; Woodsworth et al., 2015). Studies of cytokine-mediated communication, however, indicate that soluble proteins escape the T cell-target cell interface very quickly (Feinerman et al., 2010; Muller et al., 2012; Sanderson et al., 2012). An alternative strategy for boosting selectivity and efficiency would involve locally increasing the specific activity of secreted molecules. Synaptic mechanopotentiation of perforin pore formation falls into this second class of mechanisms. Synergy between force exertion and perforin activity would reduce the amount of degranulation required for each killing event and thereby limit bystander damage resulting from excessive cytolytic secretion. It would also facilitate serial killing by enabling CTLs to reserve perforin and granzyme for other targets. We expect that other cytotoxic lymphocytes will also employ this strategy.

Our results demonstrate that NMII is critical for force exertion at the IS. This is surprising given that myosin activity is dispensable for IS formation and only modestly affects synaptic architecture (Babich et al., 2012; Jacobelli et al., 2004; Yi et al., 2012). We also found that depletion of NMII reduced CTL-mediated cytotoxicity, implying that myosin dependent forces contribute to mechanopotentiation during target cell killing. Although we favor this interpretation, it must be noted that CTLs lacking NMII also exhibit delayed centrosome polarization (Liu et al., 2013). A partial polarity defect could affect cytotoxicity by altering the directionality of cytolytic secretion. Hence, at this stage we cannot attribute the killing phenotype of NMII deficient cells solely to a defect in force exertion.

Perforin pores drive target cell killing by inducing a membrane repair response that stimulates the uptake of additional perforin and granzymes (Keefe et al., 2005; Thiery et al., 2011). Although the methods used in this study assessed the effects of cellular mechanics on initial pore formation, they did not address whether force might also modulate membrane repair downstream. Membrane tension has been implicated in the regulation of both exo- and endocytosis in multiple cell types (Diz-Munoz et al., 2013). It is therefore quite plausible that CTL-induced distortions within the IS could influence membrane repair and in this manner control not only the initiation but also the progression of cytotoxicity.

F-actin accumulates in the periphery of the IS and is depleted from the center, forming a stereotyped annular pattern (Le Floc'h and Huse, 2015). Lytic granules cluster beneath the center of the F-actin ring, and it has been proposed that they release their contents primarily by fusing with the actin-free plasma membrane in this region (Stinchcombe and Griffiths, 2007; Stinchcombe et al., 2006). Using a fluorescent probe for degranulation, we found that cytolytic secretory events are not enriched in the very center of the IS, but rather in an intermediate domain that overlaps with the region of strongest force exertion. In the canonical IS, this intermediate zone is occupied by the inner aspect of the F-actin ring and clusters of integrins (Dustin et al., 2010); it therefore contains the adhesive and cytoskeletal machinery required to transmit force. Super-resolution imaging studies have demonstrated that this zone can also accommodate the formation of actin hypodense regions of plasma

membrane suitable for vesicle fusion (Brown et al., 2011; Rak et al., 2011). Accordingly, we favor a model in which degranulation occurs at the border between the central F-actin depleted area and the peripheral F-actin ring. This would enable the CTL to balance the physical requirements of exocytosis with the benefits of synaptic mechanopotentiation.

The striking spatiotemporal correlation we observed between lytic granule release and force exertion suggests that CTLs create local mechanical hotspots on the target cell surface that are particularly sensitive to perforin. Although the fluid nature of lipid bilayers generally promotes rapid equilibration of applied force, local interactions with the cytoskeleton have been shown to generate inhomogeneities in tension (Diz-Munoz et al., 2013). The idea that physical inhomogeneities of this kind could be established within dynamic and strongly adhesive interfaces, such as the IS, is quite intriguing, and represents an interesting topic for future studies.

The mechanical component of cytotoxicity could be particularly important in the context of anti-cancer immunity. Within solid tumors, cells tend to be stiffer because of enhanced cytoskeletal contractility and extracellular matrix rigidity (Paszek et al., 2005). Although increased stiffness would be expected to promote CTL-mediated killing, any advantage gained by the immune system would likely be overwhelmed by the tolerogenic signals that prevail within the tumor microenvironment (Rabinovich et al., 2007). During metastatic dissemination, however, cells from the tumor move away from this immunosuppressive milieu. In that regard, it is interesting to note that isolated cancer cells tend to be softer than their non-transformed counterparts (Guck et al., 2005; Hou et al., 2009; Xu et al., 2012). This deformability could enable them to resist immune-mediated attack when outside of the tumor microenvironment.

The intricate cytoskeletal dynamics of lymphocyte synapses include both actin flows that propagate in the plane of the interface (Bunnell et al., 2001; Grakoui et al., 1999; Ritter et al., 2015) and filopodial protrusions that can deform the surface of the target cell (Sage et al., 2012; Ueda et al., 2011). As we work to define the functional relevance of these and other structures, it will be important to consider their capacity to transmit information physically during the effector phase of lymphocyte responses. Mechanical forces are well suited for rapid and highly compartmentalized signaling within cell-cell interfaces, and as such they represent a valuable mode of intercellular communication in complex environments.

EXPERIMENTAL PROCEDURES

Additional methods may be found in Supplemental Experimental Procedures.

Micropipette-based force measurements

Stimulatory beads were prepared by coating 6 μm diameter streptavidin-coated polystyrene particles (Spherotech) with biotinylated H2-K^b-OVA and ICAM1 (1 μg/ml each) for 2 hr in 20 mM Hepes pH 7.5, 150 mM NaCl, 2% w/v BSA. Micropipettes for stimulatory beads and CTLs were prepared from borosilicate glass capillaries (1 mm OD, 0.78 mm ID, Harvard Apparatus). Imaging was carried out in an open top, environmentally controlled chamber

mounted on an inverted microscope (Nikon TE300) equipped with a 100× objective lens. The rigid CTL micropipette was attached to a motorized micromanipulator (MP285, Sutter Instruments) and the bead micropipette to manual micrometers (Thorlabs). Beads were aspirated into the tip of the calibrated micropipette by applying ~6 kPa aspiration pressure using a syringe (typically 1 ml air volume depression). 200 Pa of pressure (applied using a water reservoir) was used to aspirate a CTL into the tip of the rigid pipette. Time-lapse recordings were started just before the CTL was gently brought into contact with the bead. In general, 50 ms brightfield exposures were taken at 2 s intervals for 3–5 min using Micromanager software. The deflection of the flexible micropipette was determined by tracking the position of the bead using a customized ImageJ macro (Husson et al., 2011). Bead position was determined with a precision < 60 nm, corresponding to a precision in force better than 6 pN for probe bending stiffness k = 0.1 nN/μm.

Micropillar force assay

PDMS (Sylgard 184, Dow Corning) micropillar arrays coated with H2-K^b-OVA and ICAM1 were prepared from silicon masters as described previously (Bashour et al., 2014). All pillars were 0.7 μm in diameter, 6 μm tall, and spaced hexagonally with a 2 μm center-to-center distance. Imaging experiments were conducted using an inverted fluorescence microscope (Olympus IX-81) fitted with a 100× objective lens (Olympus). Prior to imaging, CTLs were stained with a fluorescently labeled (Alexa488 or Alexa647) anti-CD45 F_{ab} (clone 104-2, MSKCC Antibody and Bioresource Core) fragment to enable visualization of the cell membrane. They were then applied to the arrays and the cells and pillars imaged at the focal plane of the pillar tops. The CTL footprint on the pillar array (determined from the anti-CD45 F_{ab} signal) was used to identify pillars in contact with the CTL at each time point. Deflections were derived from the imaging data using custom Matlab scripts as described previously (Bashour et al., 2014).

Cellular perforation assay

24 hr prior to imaging, B16-F10 cells were plated at 10^4 cells/100 μl/well in either fibronectin-coated 96-well plates (Costar) or in 96-well flat-plates coated with polyacrylamide hydrogels (Matrigen) and fibronectin. 1 hr prior to imaging, cells were transferred into C^+ buffer (Hank's balanced salt solution (HBSS) with 10mM Hepes pH 7.2, 4 mM $CaCl_2$, 2 mM $MgCl_2$, 0.4% BSA) containing Hoechst 33342 stain (1:2000, Invitrogen). PI (100 μM final concentration) was added along with Blebbistatin (Sigma) or Latrunculin A (Sigma) as necessary. After 5 min, Hoechst and PI images were collected at 2 min intervals for 30 min using an inverted wide-field microscope (Zeiss Axiovert 200M, Metamorph acquisition software) fitted with a 5× objective lens (Zeiss). Dilutions of purified perforin in 50 μl C^- buffer (HBSS, 10mM Hepes pH 7.2, 1 mM EGTA, 0.4% BSA) were added 4 min into the imaging run. To vary tonicity, hypertonic (+ 150 mM sucrose) or hypotonic (H_2O instead of HBSS) C^+ and C^- buffers were used instead of isotonic C^+ and C^-.

CTL-target cell imaging in microwells

PDMS grids containing 50×50×25 μm wells were submerged in imaging medium and seeded with CFSE-labeled RMA-s cells that had been pulsed with 1 μM OVA. In general, individual wells contained 1–3 RMA-s cells. 100 μM PI (Life Technologies) was added to the medium to enable real time visualization of perforated cells. Then, CTLs expressing shNT or shPTEN together with CFP were added and the cells imaged using a 20× objective lens (Olympus) at 6-minute intervals for 8 hr. Brightfield, GFP, CFP, and PI images were collected at each time point. Quantification was restricted to target cells forming synapses with only one T cell during the first 6 hours of the imaging experiment. All cells in this category were scored for the time of initial IS formation and also for the first appearance of PI signal above background.

Supplementary Material

Refer to Web version on PubMed Central for supplementary material.

Acknowledgments

We thank N. Bantilan and M. Kaissar for technical support; U. Bandyopadhyay and M. Overholtzer for assistance with nitrogen cavitation; A. Gondarenko for assistance with micropillar fabrication; the Molecular Cytology Core Facility for help with imaging; the Antibody and Bioresource Core Facility for fluorescently conjugated F_{ab} fragments; S. Budhu and J. Wolchok for providing B16 cells; E. Mace and J. Orange for pHluorin-Lamp1; S. Rudensky and K. Pham for critical reading of the manuscript; and members of the Huse, Kam, M.O. Li, and G. Altan-Bonnet labs for advice. This work was supported in part by the US National Institutes of Health (R01-AI087644 to M.H., R01-AI088377 to L.C.K., PN2-EY016586 to L.C.K., and P30-CA008748 to MSKCC), the AXA-Ecole Polytechnique Chair (J.H.), LabexLaSIPS MECALEUCO (J.H.), the French National Research Agency (C.H.), the French Foundation for Medical Research (C.H.), the Geoffrey Beene Cancer Research Center (M.H.), the Starr Cancer Consortium (M.H.), and the Leukemia and Lymphoma Society (M.H.).

REFERENCES

Babich A, Li S, O'Connor RS, Milone MC, Freedman BD, Burkhardt JK. F-actin polymerization and retrograde flow drive sustained PLCgamma1 signaling during T cell activation. J Cell Biol. 2012; 197:775–787. [PubMed: 22665519]

Bashour KT, Gondarenko A, Chen H, Shen K, Liu X, Huse M, Hone JC, Kam LC. CD28 and CD3 have complementary roles in T-cell traction forces. Proc Natl Acad Sci U S A. 2014; 111:2241–2246. [PubMed: 24469820]

Beal AM, Anikeeva N, Varma R, Cameron TO, Vasiliver-Shamis G, Norris PJ, Dustin ML, Sykulev Y. Kinetics of early T cell receptor signaling regulate the pathway of lytic granule delivery to the secretory domain. Immunity. 2009; 31:632–642. [PubMed: 19833088]

Bertrand F, Muller S, Roh KH, Laurent C, Dupre L, Valitutti S. An initial and rapid step of lytic granule secretion precedes microtubule organizing center polarization at the cytotoxic T lymphocyte/target cell synapse. Proc Natl Acad Sci U S A. 2013; 110:6073–6078. [PubMed: 23536289]

Brown AC, Oddos S, Dobbie IM, Alakoskela JM, Parton RM, Eissmann P, Neil MA, Dunsby C, French PM, Davis I, et al. Remodelling of cortical actin where lytic granules dock at natural killer cell immune synapses revealed by super-resolution microscopy. PLoS Biol. 2011; 9:e1001152. [PubMed: 21931537]

Bunnell SC, Kapoor V, Trible RP, Zhang W, Samelson LE. Dynamic actin polymerization drives T cell receptor-induced spreading: a role for the signal transduction adaptor LAT. Immunity. 2001; 14:315–329. [PubMed: 11290340]

Chan CE, Odde DJ. Traction dynamics of filopodia on compliant substrates. Science. 2008; 322:1687–1691. [PubMed: 19074349]

Comrie WA, Babich A, Burkhardt JK. F-actin flow drives affinity maturation and spatial organization of LFA-1 at the immunological synapse. J Cell Biol. 2015; 208:475–491. [PubMed: 25666810]

Dai J, Sheetz MP. Mechanical properties of neuronal growth cone membranes studied by tether formation with laser optical tweezers. Biophysical journal. 1995; 68:988–996. [PubMed: 7756561]

Diz-Munoz A, Fletcher DA, Weiner OD. Use the force: membrane tension as an organizer of cell shape and motility. Trends Cell Biol. 2013; 23:47–53. [PubMed: 23122885]

Dustin ML, Chakraborty AK, Shaw AS. Understanding the structure and function of the immunological synapse. Cold Spring Harb Perspect Biol. 2010; 2:a002311. [PubMed: 20843980]

Engler AJ, Sen S, Sweeney HL, Discher DE. Matrix elasticity directs stem cell lineage specification. Cell. 2006; 126:677–689. [PubMed: 16923388]

Feinerman O, Jentsch G, Tkach KE, Coward JW, Hathorn MM, Sneddon MW, Emonet T, Smith KA, Altan-Bonnet G. Single-cell quantification of IL-2 response by effector and regulatory T cells reveals critical plasticity in immune response. Molecular systems biology. 2010; 6:437. [PubMed: 21119631]

Grakoui A, Bromley SK, Sumen C, Davis MM, Shaw AS, Allen PM, Dustin ML. The immunological synapse: a molecular machine controlling T cell activation. Science. 1999; 285:221–227. [PubMed: 10398592]

Grupp SA, June CH. Adoptive cellular therapy. Curr Top Microbiol Immunol. 2011; 344:149–172. [PubMed: 20700700]

Guck J, Schinkinger S, Lincoln B, Wottawah F, Ebert S, Romeyke M, Lenz D, Erickson HM, Ananthakrishnan R, Mitchell D, et al. Optical deformability as an inherent cell marker for testing malignant transformation and metastatic competence. Biophysical journal. 2005; 88:3689–3698. [PubMed: 15722433]

Hammer JA 3rd, Burkhardt JK. Controversy and consensus regarding myosin II function at the immunological synapse. Curr Opin Immunol. 2013

Hou HW, Li QS, Lee GY, Kumar AP, Ong CN, Lim CT. Deformability study of breast cancer cells using microfluidics. Biomedical microdevices. 2009; 11:557–564. [PubMed: 19082733]

Houk AR, Jilkine A, Mejean CO, Boltyanskiy R, Dufresne ER, Angenent SB, Altschuler SJ, Wu LF, Weiner OD. Membrane tension maintains cell polarity by confining signals to the leading edge during neutrophil migration. Cell. 2012; 148:175–188. [PubMed: 22265410]

Huang HW, Chen FY, Lee MT. Molecular mechanism of Peptide-induced pores in membranes. Phys Rev Lett. 2004; 92:198304. [PubMed: 15169456]

Hui KL, Balagopalan L, Samelson LE, Upadhyaya A. Cytoskeletal forces during signaling activation in Jurkat T-cells. Mol Biol Cell. 2015; 26:685–695. [PubMed: 25518938]

Huse M, Lillemeier BF, Kuhns MS, Chen DS, Davis MM. T cells use two directionally distinct pathways for cytokine secretion. Nat Immunol. 2006; 7:247–255. [PubMed: 16444260]

Husson J, Chemin K, Bohineust A, Hivroz C, Henry N. Force generation upon T cell receptor engagement. PloS one. 2011; 6:e19680. [PubMed: 21572959]

Ingber DE. Cellular mechanotransduction: putting all the pieces together again. FASEB J. 2006; 20:811–827. [PubMed: 16675838]

Jacobelli J, Chmura SA, Buxton DB, Davis MM, Krummel MF. A single class II myosin modulates T cell motility and stopping, but not synapse formation. Nat Immunol. 2004; 5:531–538. [PubMed: 15064761]

Keefe D, Shi L, Feske S, Massol R, Navarro F, Kirchhausen T, Lieberman J. Perforin triggers a plasma membrane-repair response that facilitates CTL induction of apoptosis. Immunity. 2005; 23:249–262. [PubMed: 16169498]

Le Floc'h A, Huse M. Molecular mechanisms and functional implications of polarized actin remodeling at the T cell immunological synapse. Cellular and molecular life sciences : CMLS. 2015; 72:537–556. [PubMed: 25355055]

Le Floc'h A, Tanaka Y, Bantilan NS, Voisinne G, Altan-Bonnet G, Fukui Y, Huse M. Annular PIP3 accumulation controls actin architecture and modulates cytotoxicity at the immunological synapse. J Exp Med. 2013; 210:2721–2737. [PubMed: 24190432]

Lee CY, Herant M, Heinrich V. Target-specific mechanics of phagocytosis: protrusive neutrophil response to zymosan differs from the uptake of antibody-tagged pathogens. J Cell Sci. 2011; 124:1106–1114. [PubMed: 21385838]

Lee MT, Hung WC, Chen FY, Huang HW. Mechanism and kinetics of pore formation in membranes by water-soluble amphipathic peptides. Proc Natl Acad Sci U S A. 2008; 105:5087–5092. [PubMed: 18375755]

Liu B, Chen W, Evavold BD, Zhu C. Accumulation of dynamic catch bonds between TCR and agonist peptide-MHC triggers T cell signaling. Cell. 2014; 157:357–368. [PubMed: 24725404]

Liu X, Kapoor TM, Chen JK, Huse M. Diacylglycerol promotes centrosome polarization in T cells via reciprocal localization of dynein and myosin II. Proc Natl Acad Sci U S A. 2013; 110:11976–11981. [PubMed: 23818610]

Lo CM, Wang HB, Dembo M, Wang YL. Cell movement is guided by the rigidity of the substrate. Biophysical journal. 2000; 79:144–152. [PubMed: 10866943]

Lopez JA, Susanto O, Jenkins MR, Lukoyanova N, Sutton VR, Law RH, Johnston A, Bird CH, Bird PI, Whisstock JC, et al. Perforin forms transient pores on the target cell plasma membrane to facilitate rapid access of granzymes during killer cell attack. Blood. 2013; 121:2659–2668. [PubMed: 23377437]

Masters TA, Pontes B, Viasnoff V, Li Y, Gauthier NC. Plasma membrane tension orchestrates membrane trafficking, cytoskeletal remodeling, and biochemical signaling during phagocytosis. Proc Natl Acad Sci U S A. 2013; 110:11875–11880. [PubMed: 23821745]

Muller AJ, Filipe-Santos O, Eberl G, Aebischer T, Spath GF, Bousso P. CD4+ T Cells Rely on a Cytokine Gradient to Control Intracellular Pathogens beyond Sites of Antigen Presentation. Immunity. 2012; 37

Natkanski E, Lee WY, Mistry B, Casal A, Molloy JE, Tolar P. B cells use mechanical energy to discriminate antigen affinities. Science. 2013; 340:1587–1590. [PubMed: 23686338]

Oakes PW, Patel DC, Morin NA, Zitterbart DP, Fabry B, Reichner JS, Tang JX. Neutrophil morphology and migration are affected by substrate elasticity. Blood. 2009; 114:1387–1395. [PubMed: 19491394]

Orr AW, Helmke BP, Blackman BR, Schwartz MA. Mechanisms of mechanotransduction. Developmental cell. 2006; 10:11–20. [PubMed: 16399074]

Ostergaard HL, Kane KP, Mescher MF, Clark WR. Cytotoxic T lymphocyte mediated lysis without release of serine esterase. Nature. 1987; 330:71–72. [PubMed: 3118212]

Paszek MJ, Zahir N, Johnson KR, Lakins JN, Rozenberg GI, Gefen A, Reinhart-King CA, Margulies SS, Dembo M, Boettiger D, et al. Tensional homeostasis and the malignant phenotype. Cancer Cell. 2005; 8:241–254. [PubMed: 16169468]

Pipkin ME, Lieberman J. Delivering the kiss of death: progress on understanding how perforin works. Curr Opin Immunol. 2007; 19:301–308. [PubMed: 17433871]

Polozov IV, Anantharamaiah GM, Segrest JP, Epand RM. Osmotically induced membrane tension modulates membrane permeabilization by class L amphipathic helical peptides: nucleation model of defect formation. Biophysical journal. 2001; 81:949–959. [PubMed: 11463637]

Rabinovich GA, Gabrilovich D, Sotomayor EM. Immunosuppressive strategies that are mediated by tumor cells. Annu Rev Immunol. 2007; 25:267–296. [PubMed: 17134371]

Rak GD, Mace EM, Banerjee PP, Svitkina T, Orange JS. Natural killer cell lytic granule secretion occurs through a pervasive actin network at the immune synapse. PLoS Biol. 2011; 9:e1001151. [PubMed: 21931536]

Ritter AT, Asano Y, Stinchcombe JC, Dieckmann NM, Chen BC, Gawden-Bone C, van Engelenburg S, Legant W, Gao L, Davidson MW, et al. Actin depletion initiates events leading to granule secretion at the immunological synapse. Immunity. 2015; 42:864–876. [PubMed: 25992860]

Sage PT, Varghese LM, Martinelli R, Sciuto TE, Kamei M, Dvorak AM, Springer TA, Sharpe AH, Carman CV. Antigen recognition is facilitated by invadosome-like protrusions formed by memory/effector T cells. J Immunol. 2012; 188:3686–3699. [PubMed: 22442443]

Sanderson NS, Puntel M, Kroeger KM, Bondale NS, Swerdlow M, Iranmanesh N, Yagita H, Ibrahim A, Castro MG, Lowenstein PR. Cytotoxic immunological synapses do not restrict the action of

interferon-gamma to antigenic target cells. Proc Natl Acad Sci U S A. 2012; 109:7835–7840. [PubMed: 22547816]

Stinchcombe JC, Griffiths GM. Secretory mechanisms in cell-mediated cytotoxicity. Annual review of cell and developmental biology. 2007; 23:495–517.

Stinchcombe JC, Majorovits E, Bossi G, Fuller S, Griffiths GM. Centrosome polarization delivers secretory granules to the immunological synapse. Nature. 2006; 443:462–465. [PubMed: 17006514]

Thiery J, Keefe D, Boulant S, Boucrot E, Walch M, Martinvalet D, Goping IS, Bleackley RC, Kirchhausen T, Lieberman J. Perforin pores in the endosomal membrane trigger the release of endocytosed granzyme B into the cytosol of target cells. Nat Immunol. 2011; 12:770–777. [PubMed: 21685908]

Ueda H, Morphew MK, McIntosh JR, Davis MM. CD4+ T-cell synapses involve multiple distinct stages. Proc Natl Acad Sci U S A. 2011; 108:17099–17104. [PubMed: 21949383]

Wakatsuki T, Schwab B, Thompson NC, Elson EL. Effects of cytochalasin D and latrunculin B on mechanical properties of cells. J Cell Sci. 2001; 114:1025–1036. [PubMed: 11181185]

Woodsworth DJ, Dunsing V, Coombs D. Design Parameters for Granzyme-Mediated Cytotoxic Lymphocyte Target-Cell Killing and Specificity. Biophysical journal. 2015; 109:477–488. [PubMed: 26244730]

Xu W, Mezencev R, Kim B, Wang L, McDonald J, Sulchek T. Cell stiffness is a biomarker of the metastatic potential of ovarian cancer cells. PloS one. 2012; 7:e46609. [PubMed: 23056368]

Yi J, Wu XS, Crites T, Hammer JA 3rd. Actin retrograde flow and actomyosin II arc contraction drive receptor cluster dynamics at the immunological synapse in Jurkat T cells. Mol Biol Cell. 2012; 23:834–852. [PubMed: 22219382]

Highlights

- T cell cytotoxicity correlates with the exertion of mechanical force
- Force exertion is associated with enhanced perforin pore formation on the target cell
- Cell tension promotes perforin pore formation
- Cytotoxic T cells spatiotemporally coordinate force exertion and perforin release

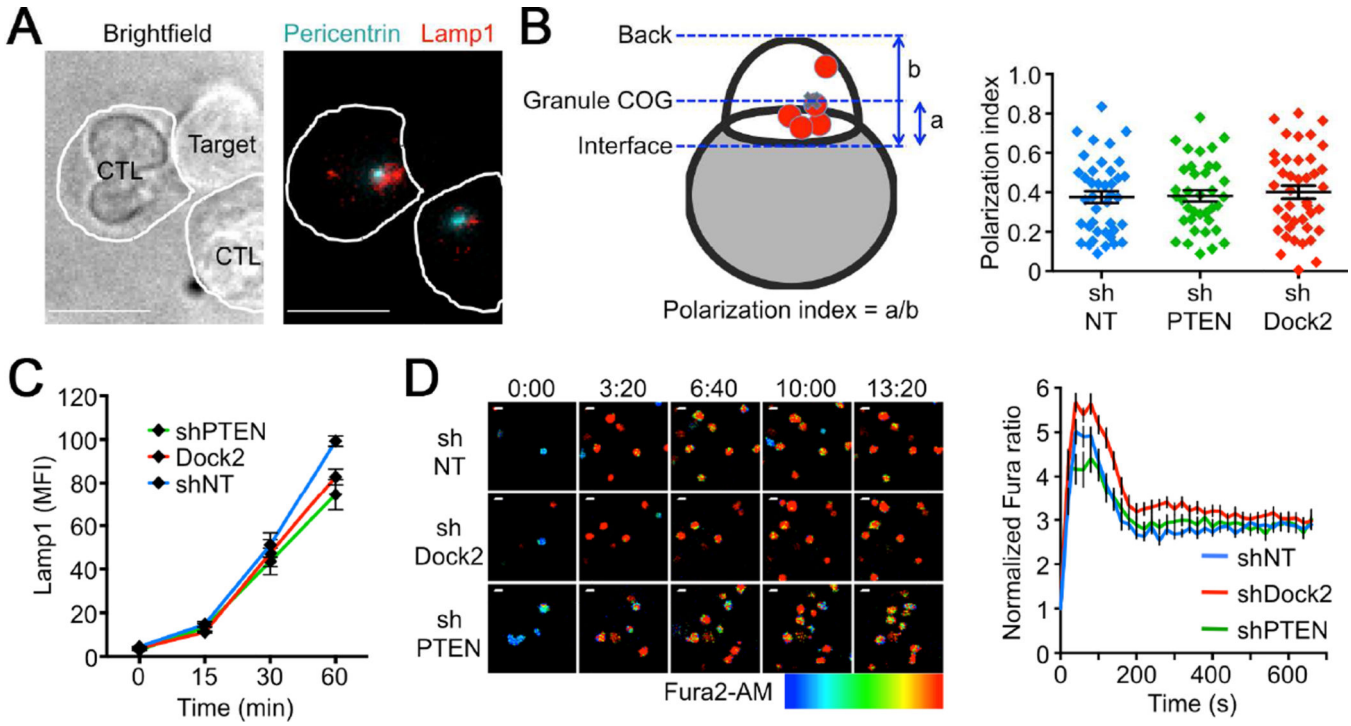

Figure 1. PTEN and Dock2 are not required for lytic granule polarization and Ca^{2+} flux

(A–B) OT1 CTLs expressing the indicated shRNAs were mixed with OVA-loaded EL4 cells, fixed, and stained for pericentrin and Lamp1 to visualize the centrosome and lytic granules, respectively. (A) Left, brightfield image of a representative CTL-target cell conjugate. Right, corresponding fluorescence image, with white lines indicating CTL boundaries. (B) Left, polarization index was calculated using the center of gravity (COG) of the lytic granules (see Supplemental Experimental Procedures). Right, quantification of lytic granule polarization index ($n \geq 37$ per sample). ns, not significant (two-tailed Student's T-test). (C) OT1 CTLs expressing the indicated shRNAs were mixed with OVA-loaded EL4 cells and degranulation assessed by surface exposure of Lamp1. (D) CTLs expressing the indicated shRNAs were loaded with Fura2-AM and imaged on glass surfaces coated with H2-K^b-OVA and ICAM1. Left, representative time-lapse montages of CTLs contacting the stimulatory surfaces. Images are pseudocolored with warmer colors (e.g. orange, red) indicating higher concentrations of intracellular Ca^{2+}. Time in MM:SS is indicated above the montages. Right, mean normalized Fura ratio (see Supplemental Experimental Procedures) graphed against time. $n \geq 21$ cells per sample. All scale bars = 10 μm. Error bars denote standard error of the mean (SEM). Data are representative of at least two independent experiments. See also Figure S1.

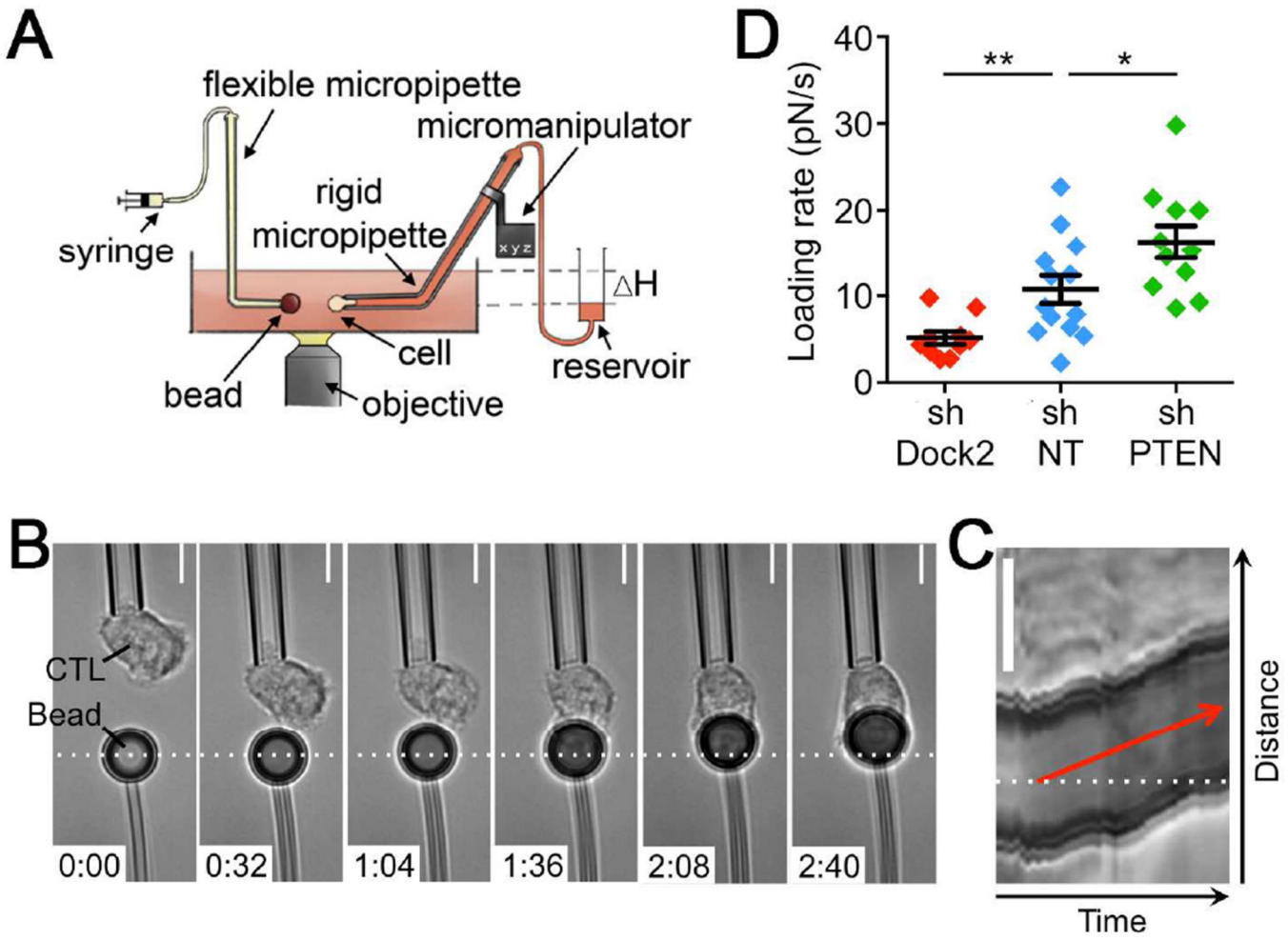

Figure 2. PI3K signaling controls force exertion perpendicular to the IS

(A) Schematic diagram of the micropipette-based system. (B) Time-lapse montage of a representative micropipette experiment. Dashed white line denotes the initial position of the bead. Time is indicated in M:SS in the bottom left corner of each image. (C) Kymograph of the experiment shown in B. The loading rate can be derived from the slope of the red line. (D) Average loading rate during the pulling phase of the response, calculated for cells expressing the indicated shRNAs. Error bars denote SEM. $n \geq 10$ cells per condition. *, $P < 0.05$, **, $P < 0.01$, calculated by two-tailed Mann-Whitney test. All scale bars = 5 μm. Data are representative of at least two independent experiments. See also Movie S1.

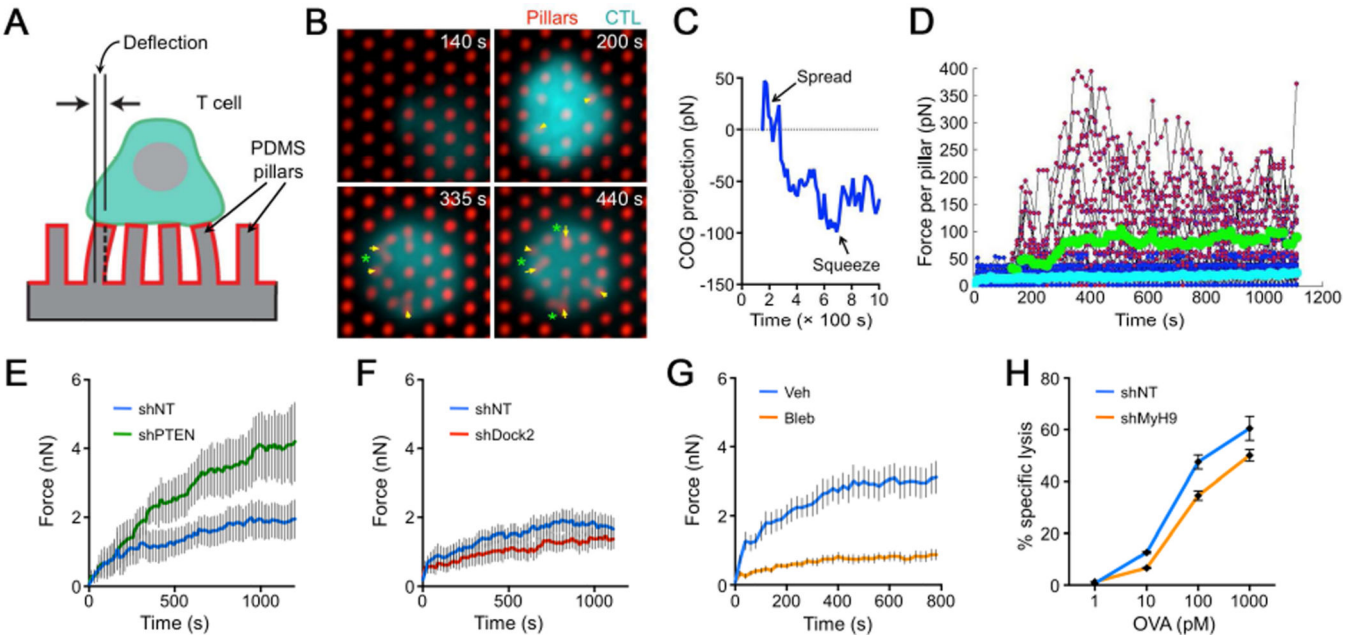

Figure 3. PI3K signaling and NMII control force exertion parallel to the IS

(A) Schematic diagram of the micropillar system. (B–F) CTLs expressing shNT, shDock2, or shPTEN were imaged on stimulatory micropillar arrays. (B) Time-lapse montage of a representative CTL-micropillar interaction. Time is indicated in the top right corner of each image. Large pillar deflections are indicated by yellow arrows. Green asterisks denote "hotspots" of strong force exertion. (C) Average projection of pillar deflections along the line connecting each pillar to the cell center of gravity (COG projection) was determined for the CTL shown in B and plotted against time. (D) Aggregate plot of instantaneous force per pillar exerted by the CTL in B, graphed against time. Pink dots denote pillars in contact with the cell, and blue dots denote pillars outside of the interface. Average force per pillar within the interface is shown in green, and background force per pillar in cyan. (E–F) Total force exertion against the pillar array graphed versus time for CTLs expressing the indicated shRNAs. n ≥ 6 cells per sample. (G) CTLs treated with 50 μM blebbistatin (Bleb) or vehicle control (Veh) were imaged on stimulatory micropillar arrays. Total force exertion against the array is graphed as in E. (H) CTLs expressing the indicated shRNAs were mixed 1:1 with OVA-loaded RMA-s cells. Specific lysis is graphed as a function of OVA concentration. All error bars denote SEM. Data are representative of at least 2 independent experiments. See also Figure S2 and Movie S2.

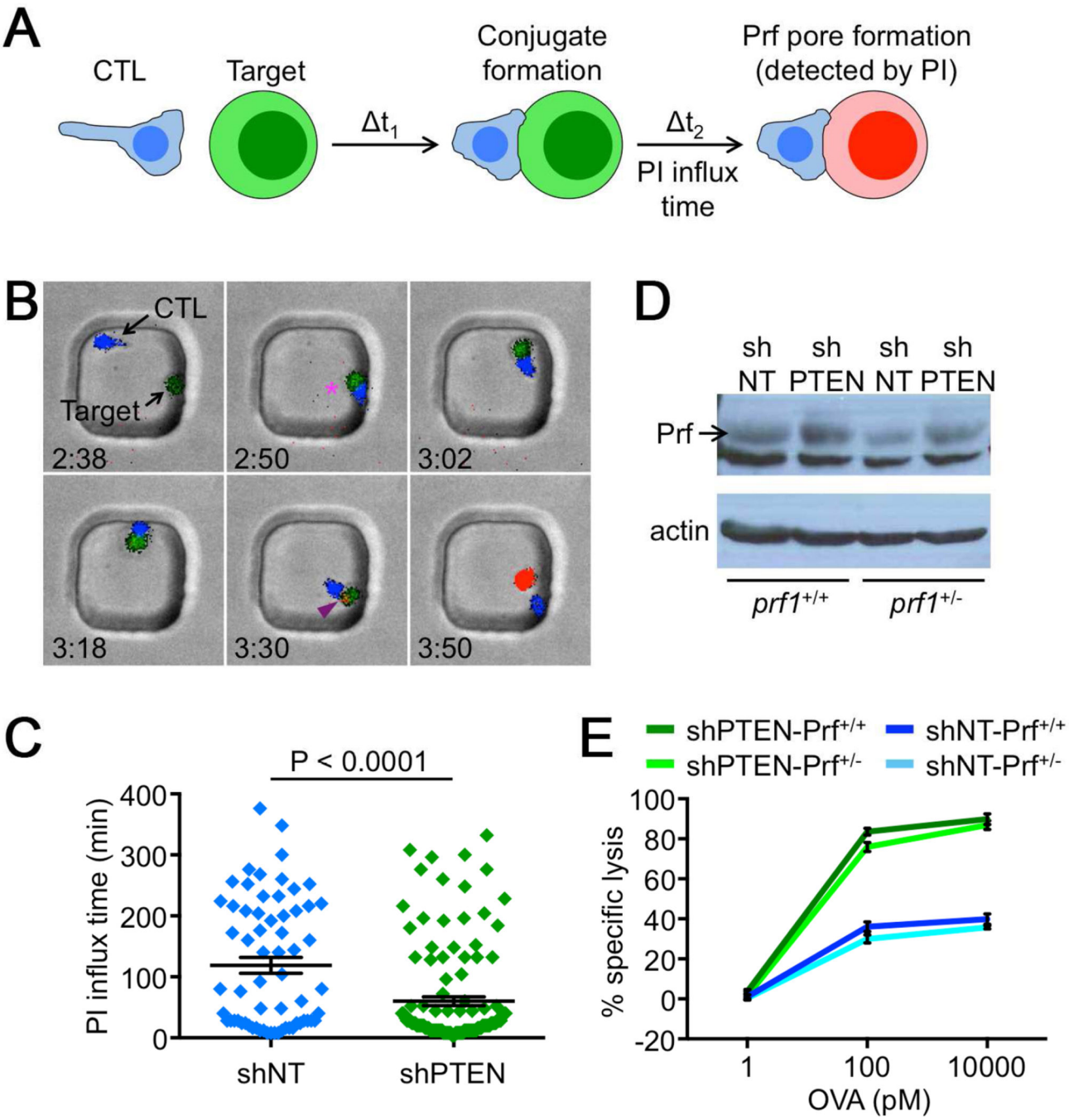

Figure 4. PTEN deficiency enhances perforin pore formation

(A) Schematic diagram showing perforin pore detection by PI. (B–C) CTLs expressing shNT or shPTEN together with cyan fluorescent protein (CFP) were mixed with carboxyfluorescein succinimidyl ester (CFSE)- labeled, OVA-loaded RMA-s cells and imaged in PDMS microwells in the presence of 100 μM PI. (B) Time-lapse montage of a representative microwell showing conjugate formation (magenta asterisk), and PI influx (purple arrowhead). Time is indicated in H:MM in the bottom left corner of each image. (C) Time between conjugate formation and PI influx (PI influx time) quantified for shNT and

shPTEN expressing CTLs. Error bars denote SEM. n ≥ 65 conjugates per sample. P-value calculated by two-tailed Mann-Whitney test. (D) Perforin (Prf) expression in the indicated CTLs was analyzed by Western blot. Actin served as a loading control. (E) $prf1^{+/+}$ and $prf1^{+/-}$ CTLs expressing the indicated shRNAs were mixed 1:1 with OVA-loaded RMA-s cells. Specific lysis is graphed as a function of OVA concentration. Data are representative of at least 2 independent experiments. See also Movie S3.

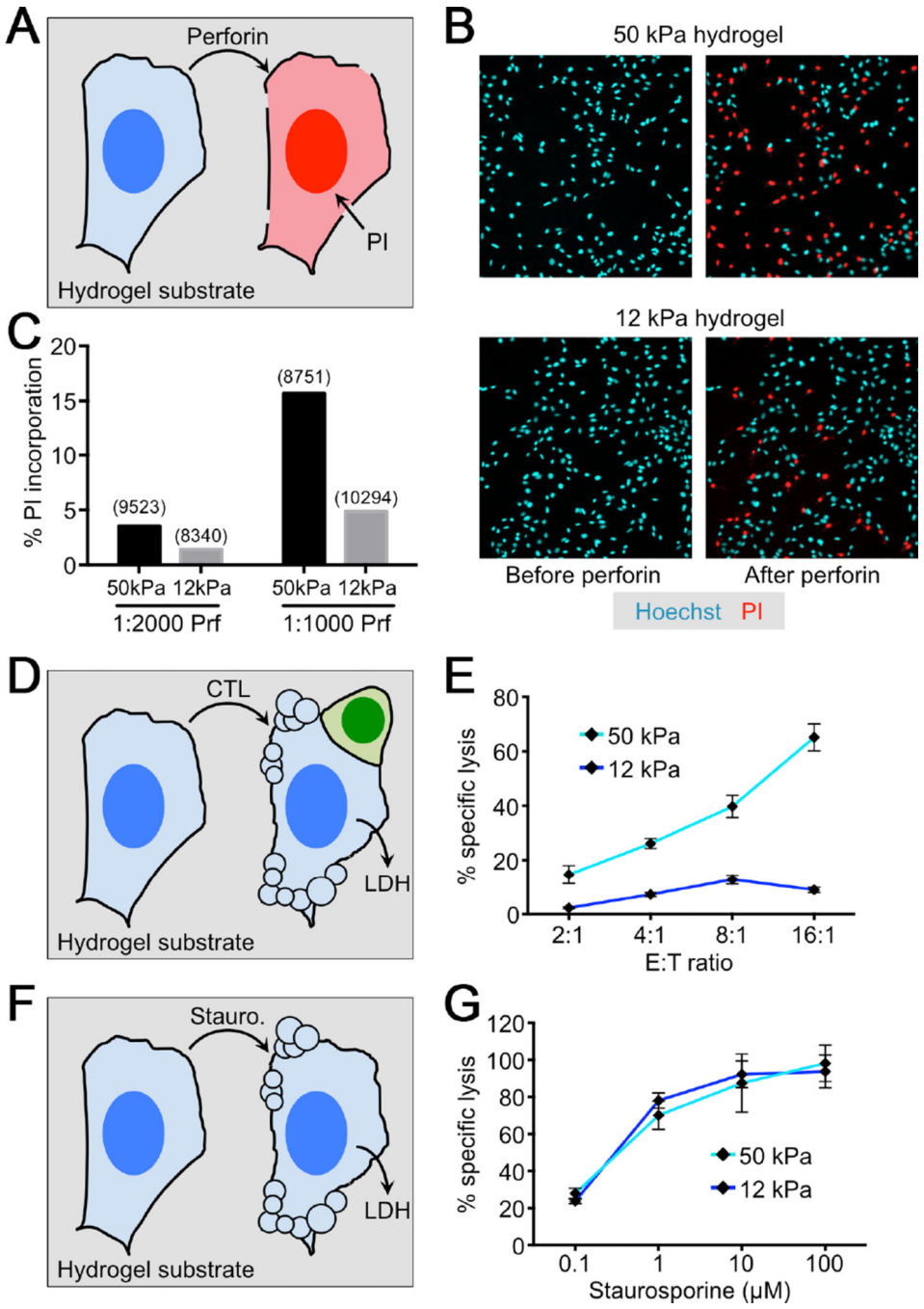

Figure 5. Cell tension promotes perforin pore formation and CTL-mediated killing

(A–C) B16 cells were cultured overnight on stiff (E = 50 kPa) or soft (E = 12 kPa) hydrogels, stained with Hoechst 33342, and treated with the indicated dilutions of perforin (1:1000 ≈ 1 μg/ml final concentration) in the presence of 100 μM PI. (A) Schematic diagram of the perforation assay. (B) Representative images before and after perforin treatment on both stiff (top) and soft (bottom) hydrogels. Perforated cells were identified by their PI^+ nuclei. (C) Quantification of a representative perforation experiment on hydrogels. Total cell counts are shown in parentheses above each bar. (D) Schematic diagram of a B16

killing assay on hydrogel substrate. (E) OT1 CTLs were added to OVA-loaded B16 cells grown on stiff or soft hydrogels. Specific lysis was quantified by LDH release at the indicated effector to target (E:T) ratios. (F) Schematic diagram of staurosporine-induced apoptosis on hydrogel substrate. (G) B16 cells grown on stiff or soft hydrogels were exposed to the indicated concentrations of staurosporine. Apoptosis was quantified by LDH release. Error bars denote SEM. Data are representative of at least 2 independent experiments. See also Figures S3–S5 and Movies S4 and S5.

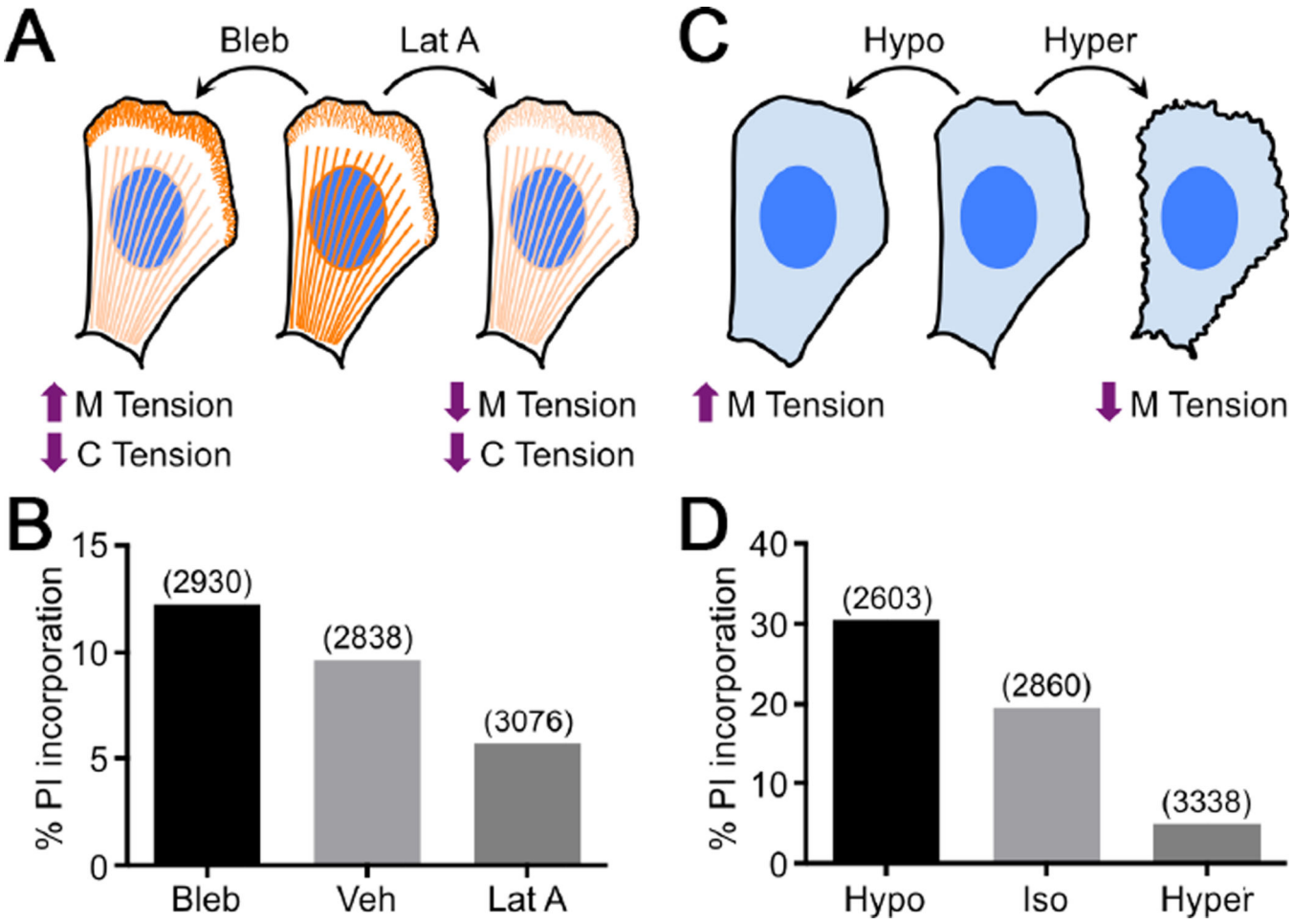

Figure 6. Membrane tension potentiates perforin pore formation

(A) Diagram schematizing the effects of blebbistatin (Bleb) and latrunculin A (Lat A) on cortical (C) and membrane (M) tension. Lamellipodial F-actin and stress fibers are indicated in orange. (B) B16 cells cultured on plastic were treated with perforin (1:1000 dilution) in the presence of 100 μM PI and either 100 μM Bleb, 7.5 μM Lat A, or vehicle control (Veh) as indicated. Perforation was quantified by PI incorporation. (C) Diagram schematizing the effects of hypotonic (Hypo) or hypertonic (Hyper) medium on membrane tension. (D) B16 cells cultured on plastic were treated with perforin (1:1000 dilution) in the presence of 100 μM PI either in isotonic (Iso), hypotonic, or hypertonic medium as indicated. Perforation was quantified by PI incorporation. In B and D, total cell counts are shown in parentheses above each bar. Data are representative of 3 independent experiments. See also Figure S4.

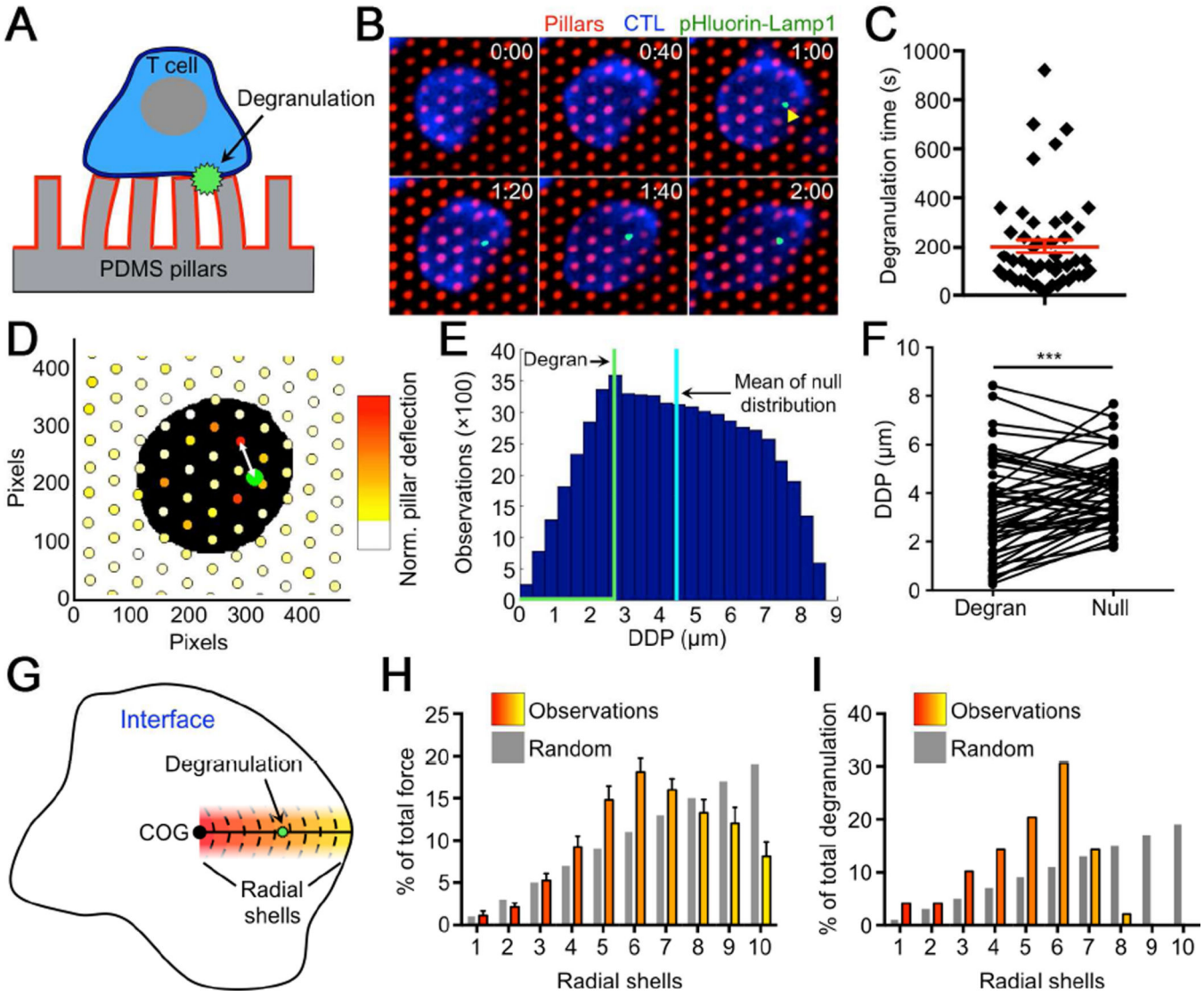

Fig. 7. Degranulation is spatiotemporally correlated with force exertion at the IS

(A) Diagram schematizing fluorescent detection of degranulation during a micropillar experiment. (B–F) CTLs expressing pHluorin-Lamp1 were imaged on stimulatory micropillar arrays. (B) Representative time-lapse montage showing pillar deflections during a degranulation event (indicated by the yellow arrowhead). Time is indicated in M:SS in the top right corner of each image. (C) Graph of the offset time between contact formation and degranulation (degranulation time). (D) Graphical representation of the pillar array in B, with the degranulation position depicted as a green circle and the cell envelope at the moment of degranulation shown in black. Pillars are color-coded based on their average deflection during the degranulation. Warmer colors (e.g. orange, red) denote stronger deflections. The DDP for this degranulation is indicated by the double-headed white arrow. (E) Histogram plot derived from the experiment in B showing the DDP for each position in the CTL interface. The mean value for the distribution is denoted by the vertical cyan line. The vertical green line indicates the DDP for the degranulation itself. (F) DDPs of

degranulation (Degran) were compared to the mean values of their paired null distributions. ***, $P < 0.001$, calculated by two-tailed paired T-test. (G) Schematic diagram of the CTL-array interface showing the radial shells used for spatial analysis. (H–I) The radial distribution of total force exertion (H) and degranulation position (I) in degranulating cells. Color-coding of the bars corresponds to the shells shown in G. Gray bars indicate the spatial distribution that would be expected by chance (outer shells are larger than inner ones). All error bars denote SEM. For C, F, and I, n = 49 degranulation events pooled from three independent experiments. See also Figure S6.